ISSN 1069-3513, Izvestiya, Physics of the Solid Earth, 2023, Vol. 59, No. 5, pp. 717–732. © Pleiades Publishing, Ltd., 2023.
Russian Text © The Author(s), 2023, published in Fizika Zemli, 2023, No. 5, pp. 62–78.

Staging of Occurrence of Seismicity Anomalies before Earthquakes in Kamchatka, Japan and Iceland

V. B. Smirnov[a, b, *] and A. A. Petrushov[a, b]

[a] Physics Department, Moscow State University, Moscow, 119991 Russia
[b] Schmidt Institute of Physics of the Earth, Russian Academy of Sciences, Moscow, 123242 Russia
*e-mail: vs60@mail.ru

Received April 7, 2023; revised April 16, 2023; accepted April 20, 2023

Abstract—The paper presents the results of a study showing that anomalies in the seismic regime parameters before earthquakes of various magnitudes occur in stages. The occurrence in stages means the correlation between the times of formation and development of anomalies in various seismic regime parameters. Earthquakes in regions with two general types of tectonics are selected for analysis: in the subduction zone (Kamchatka and Japan) and in the rift zone (Iceland). The selection of regions is primarily based on the availability and quality of regional seismic catalogs. GR *b*-value and the composite parameter known as the *RTL* are used as the seismic regime parameters. The detection of spatiotemporal anomalies before the selected earthquakes is based on the known "precursory patterns" of the seismic regime parameters. Comparing the durations of the detected anomalies shows that the anomalies of *b*-value generally occur earlier than the *RTL* anomalies. Possible reasons why the anomalies occur in stages are suggested. In the vicinity of the studied earthquakes, a change in the seismogenic rupture concentration parameter within the corresponding seismic cycles is also estimated. Comparing the times at which the detected seismic regime anomalies occur with the values of the seismogenic rupture concentration parameter corresponding to these times shows that the formation of seismic regime anomalies occurs at a stage when the system of seismogenic ruptures accumulated during the seismic cycle has almost reached its critical value.

Keywords: seismic regime, seismic anomalies, occurrence in stages

DOI: 10.1134/S1069351323050129

INTRODUCTION

Anomalies of seismicity are the most reliably detectable geophysical effects associated with earthquake preparation processes. The vast majority of currently available prognostic algorithms analyze the data from earthquake catalogs. On the one hand, this is due to the fact that the processes of strong earthquake source preparation are associated with a gradual development of failures at smaller scales. On the other hand, seismic catalogs contain data with the required level of spatial detail for entire earthquake generation areas. Detecting the spatiotemporal structure of a prognostic anomaly in the source region of the strongest earthquakes with a typical source size of 100 km (magnitude 8 earthquakes) requires a 10–20 km level of detail in the initial geophysical observation data. As for weaker, but practically dangerous earthquakes with a source size of 30 km (magnitude 6.5), the detection requires a 3–5 km level of detail in the observation data. This spatial resolution is provided by current seismic catalogs based on data from world or regional seismic networks, which everywhere have an accuracy of locating epicenters of events no worse than 5 km and depths, as a rule, no worse than 10 km. The level of spatial detail in ground observations of other geophysical fields (deformation field, magnetic field, gravity field, etc.) depends on the average distance between the respective geophysical observatories, which is usually hundreds of kilometers. This is one or one and a half orders of magnitude worse than the resolutions of seismic catalogs. A number of remote sensing satellite techniques for measuring geophysical fields provide the necessary spatial resolution of less than ten to the first tens of kilometers, but the effective sensitivity of almost all of these techniques is still inadequate to detect anomalies caused by the preparation processes of even the strongest earthquakes.

The world practice of prognostic studies has revealed a number of statistical seismic regime parameters whose abnormal changes are considered to be indicators of earthquake preparation processes. First of all, they include the characteristics of the energy "spectrum" of seismicity: Gutenberg-Richter *b*-value, various characteristics of seismic activity; characteristics of the spatial, temporal or spatiotemporal density of released seismic energy; parameters of earthquake clustering and interaction (Sobolev, 1993; Zavyalov, 2006; Sobolev and Ponomarev, 2003; Panza et al., 2022). For some of these parameters, "precursory patterns" (i.e., characteristic temporal forms of anomalies and their distribution in space in the earthquake preparation region) are known.

This paper presents the results of a study showing that anomalies of seismicity before relatively strong earthquakes occur in stages. The occurrence in stages means the correlation between the times of formation and development of anomalies of various parameters of seismicity. We have selected earthquakes in regions with two general types of tectonics: in the subduction zone (Kamchatka and Japan catalogs) and in the rift zone (Iceland catalog). We have decided on these regions primarily due to the availability and quality of seismic catalogs.

It should be noted that we do not intend to develop or modify prognostic algorithms and their practical applications. At this point, the study aims to compare the spatiotemporal regions in which seismic anomalies occur and to find out if there are any patterns in the evolution of the anomalies over time. We have selected only those earthquakes before which reliable anomalies of seismicity are detected, and have not considered the question of when and why anomalies are observed and when they are not. In the future, as we accumulate more of this information, we plan to classify it in order to find out whether or not there are specific features of the occurrence of anomalies in stages. In selecting the earthquakes of the regions under study, we have considered not only our own research findings, but also literature data on the presence of prognostic seismic regime anomalies before the earthquakes in question.

CHARACTERISTICS OF THE SEISMICITY PARAMETERS USED

Anomalies of seismicity preceding strong earthquakes, which are the subject of the present study, belong to the so—called physical precursors of earthquakes (Sidorin, 1992; Sobolev, 1993). Their origin is associated with the development of failures in the local region of the lithosphere, which eventually results in this region being destroyed by the source of the earthquake. There are several known scenarios for the development of such failures leading to a strong earthquake—qualitative models of earthquake preparation. Two main models were proposed almost simultaneously in the early 1970s in the USA—the dilatancy-diffusion model, and in the USSR—the avalanche unstable fracturing formation (AUF) model (Miachkin et al., 1972; Schotz et al., 1973; Mjachkin et al., 1975). Both models explained the properties of pre—earthquake geophysical field anomalies known at the time. Later, these models were modified and developed theoretically and statistically. Both models have their strengths and weaknesses and still compete in explaining the effects found in the evolution of seismicity.

The earthquake preparation models provided a set of seismicity parameters that can be statistically estimated from earthquake catalog data. The AUF and similar models imply a gradual increase in the size of seismogenic ruptures due to the accumulation and coalescence of smaller ruptures when they reach a critical concentration where the anomalous stress fields caused by the rupture formation overlap. Therefore, the parameters reflecting the development of an earthquake preparation process include characteristics of earthquake source concentration, ratios between the frequencies of earthquakes of various energies (magnitudes), characteristics of the influence of previous earthquakes on subsequent ones, characteristics of the spatiotemporal connectivity of earthquake sequences, etc. Below are brief descriptions of the three parameters selected for this paper.

Gutenberg–Richter b-value

The classic parameter of seismicity is the exponent of the energy "spectrum" of seismicity. It characterizes the ratio of probabilities for earthquakes of various energies (magnitudes). Anomalies of b-value, observed before strong earthquakes, are among the most reliable indicators of instability forming in the strong earthquake preparation region, which are most often used in prognostic algorithms. The "precursory pattern", i.e., a decrease in the b-value (sometimes preceded by its slight increase) before a strong earthquake, is explained by the scenario of accumulation and coalescence of seismogenic ruptures leading to the formation of larger seismic events. In seismic statistics, this is manifested by an increase in the relative proportion of stronger earthquakes, which results in a decrease in the b-value. To estimate the b-value, we apply a technique based on maximum likelihood estimation, modified for the case of truncated distributions of earthquakes by magnitude (Smirnov and Ponomarev, 2020[1]).

RTL Parameter

The composite RTL parameter proposed by G.A. Sobolev (Sobolev et al., 1996) is essentially a total "seismic release" calculated for each selected point in space and each selected moment in time, statistically weighted with the distance and time from the earthquake that occurred to the selected point and selected moment in time. The contribution of the magnitude of the earthquake that occurred is accounted for by the exponent to which the size of its source is raised in the summation. Different values of the exponents can be correlated with the summation of different characteristics of "seismic release": the value of exponent 1— summation (accumulation) of movements in the sources of earthquakes, 2—summation

[1] https://cloud.mail.ru/public/rfq3/CNDPQRZ7r

(accumulation) of areas of ruptures, 3—summation of energies (energy release). The distance between the point in space and the moment in time being calculated and the point and time of the source of the earthquake that occurred is accounted for by exponential factors. The "pattern" of the precursory anomaly is a decrease in the *RTL* (seismic quiescence), followed by its increase (foreshock activation) (Sobolev and Ponomarev, 2003). Both effects—quiescence and activation—have a physical explanation under the AUF concept of a strong earthquake source preparation process (Sobolev, 2019). The *RTL* algorithm is quite widely used both in Russia and abroad (Nagao et al., 2011; Proskura et al., 2019; Zhang and Huang, 2022). The *RTL* parameter can also be regarded as a characteristic (function) of earthquake influence (Smirnov and Ponomarev, 2020).

The *RTL* parameter is estimated with authoring software, the first version of which was used in the above–mentioned pioneer work by (Sobolev et al., 1996). The latest, most advanced version was written in 2022 by (Petrushov and Smirnov, 2022) and is currently supported[2].

Seismogenic Rupture Concentration Parameter

The seismogenic rupture concentration parameter was introduced in laboratory studies by S.N. Zhurkov and V.S. Kuksenko (Zhurkov et al., 1977) and applied to the seismicity scale by G.A. Sobolev and A.D. Zavyalov (Sobolev and Zavyalov, 1980). It is used in prognostic studies in combination with other characteristics to construct prognostic maps of regions with high probability of expected earthquakes (Zavyalov, 2006). It is essentially a ratio of the mean distance between earthquake sources to the size of the sources. It is a measure of how close the failure regime is to the avalanche–like increase conditions. When the distance between the ruptures formed by a given time is much greater than their size, the ruptures do not "interact"—the stress fields distorted by the ruptures do not overlap. When, due to an accumulation of ruptures and an increase in their concentration, the distance between ruptures becomes comparable to their size, the perturbations of the local stress fields near the peaks of properly oriented ruptures begin to overlap, which increases the probability that the bridge between the ruptures will fail and form a less stable rupture of a larger size. According to the AUF concept, this state represents the transition of the failure process to the avalanche–like stage. The seismogenic rupture concentration parameter was estimated according to the standard technique (Zavyalov, 2006).

[2] https://gitlab.com/Mr.Brain/PyRTL

SPECIFIC FEATURES OF IMPLEMENTING ALGORITHMS FOR ESTIMATING THE PARAMETERS OF SEISMICITY

The parameters are calculated in spatiotemporal windows, and the results are presented as distribution maps of parameter values for each selected moment in time. Changes in the parameters over time are given for the selected local spatial regions.

According to the papers by (Sobolev et al., 1996; Sobolev and Ponomarev, 2003), the *RTL* parameter is calculated as the product of three functions:

$$RTL = RTL, \tag{1}$$

$$R(x,y,z,t) = \sum_i \exp\left(-\frac{r_i}{r_0}\right) - R_s, \tag{2}$$

$$T(x,y,z,t) = \sum_i \exp\left(-\frac{t_i}{t_0}\right) - T_s, \tag{3}$$

$$L(x,y,z,t) = \sum_i \left(\frac{l_i}{l_0}\right)^p - L_s. \tag{4}$$

The *RTL* is calculated at a certain point in space with the coordinates (x,y,z) and at a certain moment in time t. Here: r_i is the distance from the i–th earthquake to the point (x,y,z); t_i is the time interval from the i–th earthquake to the specified time t; l_i is the size of the i–th earthquake source. The r_0, t_0 and l_0 factors are parameters of the algorithm, they are chosen empirically in the process of adapting the algorithm to the regional seismicity characteristics and the magnitude range of the earthquakes studied according to the maximum of the detected anomaly. The adjustments R_s, T_s and L_s are introduced to remove straight line trends in time for each of the three functions.

The *RTL* algorithm is implemented as a PyRTL software package in Python 3 using modern data processing and visualization libraries (including numpy, scipy, matplotlib). The technique for processing the time dependences of the *RTL* parameter greatly affects the stability of the algorithm, and special attention was paid to the choice of the data processing method. The *RTL* parameter is calculated for a given moment in time t in several steps.

a) Calculating the initial values of the R, T, L functions. In this step, the three functions are calculated separately according to formulas (2), (3), (4). The R and L values are calculated from data of all earthquakes that have occurred by the moment in time t. These functions do not decrease monotonically with time as more and more positive terms are added to them. The T function behaves non–monotonically, since the effect of earthquakes that have already occurred decreases exponentially with time. All the three functions are calculated at a given point in space, and account for events whose epicenters are located in a certain vicinity of the given point. To speed up the operation of the algorithm, we limited the calculation area by a radius several times larger than the r_0 value. A similar time interval limit (several times larger than the t_0 value) was applied for the T function. These assumptions are justified by the exponential weighting factors in formulas (2) and (3).

b) Removing the linear trend. After the functions R, T, and L are calculated at each point in space, their linear trend is removed in time. The result is a time series with a zero mean.

c) Calculating and normalizing the *RTL*. The values of the R, T, and L functions obtained in the previous step without a linear trend are multiplied together to form the *RTL* parameter. The *RTL* is then normalized by its standard deviation, calculated over the entire time series since the start of the construction. The final values are *RTL* time series in units of their standard deviation.

As noted above, a decrease in the values of the *RTL* parameter relative to the long–term background level in a spatiotemporal region is characteristic of the seismic quiescence stage, while the subsequent recovery to or above the background level occurs during the foreshock activation stage. This behavior of the parameter is considered an anomaly (in some cases, only a drop below the background level is taken as an anomaly). It should be noted that in recent years, there has been a growing interest in analyzing the algorithm and its parameters using machine learning techniques (Proskura et al., 2019; Kali et al., 2021). The authors of the latter paper considered the possibility of applying neural network classifier models in which the values of the *RTL* function are used as input data. The model trained in this way is as effective as the best of the 7 models considered in the paper by (Kali et al., 2021).

The specifics of constructing estimates of the b-value are described in detail in the paper by (Smirnov and Ponomarev, 2020). The b-value and its error σ_b are often determined using the maximum likelihood estimation for an ungrouped data sample (Aki, 1965; Kendall and Stuart, 1973):

$$b = \frac{1}{\bar{M} - M_1}\frac{1}{\ln 10}, \qquad (5)$$

$$\sigma_b = b\big/\sqrt{N}, \qquad (5')$$

where: $\bar{M}$ is the mean magnitude; M_1 is the minimum magnitude in the sample; N is the number of seismic events used to estimate b.

Estimate (5) corresponds to the true b-value under the assumption that the magnitude values are not bounded from above. The $\bar{M}$ estimate as a mean over a finite sample turns out to be biased because the sample turns out to be actually censored from above by some magnitude. In this case, the mean $\bar{M}$ value for this sample will be less than the mathematical expectation, which means that estimate (5) will give an overestimate of b. Therefore, when calculating b-value, we use the following maximum likelihood estimation for the censored sample:

$$\frac{1}{b_{\min}} = \frac{1}{b_{\max}} + \frac{\Delta M \ln 10}{10^{b_{\min}\Delta M} - 1}, \quad \Delta M = M_2 - M_1, \qquad (6)$$

where M_2 is the upper threshold of magnitude in the sample, the $b_{\max}$ value is calculated by formula (5), the $b_{\min}$ value is obtained from the solution of algebraic equation (6). The derivation of equation (6), the history of the matter, and the description of applications can be found in the paper by (Smirnov and Ponomarev, 2020).

Considering (5) and (6) as estimates of b-value from above and below, respectively, we calculate the final b value as their semi–sum:

$$b = \frac{b_{\max} + b_{\min}}{2}. \qquad (7)$$

The Z parameter (Z criterion) is often used to detect anomalies in b-value (Saltykov and Konovalova, 2010; Saltykov et al., 2013). The Z value is a measure of the statistical significance of deviations of b-value from its long–term values. b-value is calculated in the large window (reflecting its background values) and in the working window reflecting the current value, and then the Z value is calculated as follows:

$$Z = \frac{b_2 - b_1}{\sqrt{\sigma_1^2 + \sigma_2^2}}, \qquad (8)$$

where b_1 and b_2 are the values of the recurrence curve slopes in the background and working windows, respectively; σ_1^2 and σ_2^2 are the dispersions (squares of errors) of the b_1 and b_2 estimates.

The values of the seismogenic rupture concentration parameter were calculated according to the formula:

$$K_{\mathrm{sr}} = \frac{\mu^{-\frac{1}{3}}}{l_{\mathrm{av}}}, \qquad (9)$$

where: μ is the volume density (concentration) of ruptures; $l_{\mathrm{av}} = \frac{1}{n}\sum_{i=1}^{n} l_i$ is the mean size of the rupture in a given area; n is the number of events in a given area (Zavyalov, 2006). From the start, we set a threshold for the magnitude of the events to be analyzed. Each time an event above the specified energy threshold occurred, the calculation was reset. Such a technique for calculating K_{sr} is conditioned by the notions of the seismic cycle and is described in the paper by (Zavyalov, 2006). The seismically active regions under consideration were divided into elementary seismically active cells with the area dimensions ΔX, ΔY and the depth size ΔH. For each elementary volume, we calculated the values of the K_{sr} parameter as a function of time. We smoothed out possible errors in determining the hypocenters by overlapping half the cells (Zavyalov, 2006).

From a physical point of view, the failure concentration criterion reflects the loss of stability of the fracture system in the stress field (Zavyalov, 2006; Smirnov and Ponomarev, 2020). Fractures lose stability, grow exponentially and merge into larger fractures when they are located close enough to each other, i.e., when there is quite a high concentration of fractures in some spatial region. The process is accompanied by a decrease in the value of the K_{sr} parameter over time.

The critical K_{sr}^{*} value, at which the main earthquake occurs, varies for different seismically active regions. In case of nonuniform and fractal distribution of earthquakes in space, the K_{sr}^{*} value also depends on the size of the cell for which the estimate is made according to formula (9) (Smirnov and Zavyalov, 1996).

The calculation of the seismogenic rupture length included in (9) is based on the correlation between the source size and the earthquake magnitude (or energy class):

$$\log l_i = \alpha M_i + c, \tag{10}$$

where M_i is the energy characteristic of the earthquake (magnitude or energy class). The α and c factors in equation (10) were selected according to the recommendations given in the paper by (Smirnov and Ponomarev, 2020), based on Sadovsky's formula (Sadovsky et al., 1983) and generally accepted correlations between earthquake magnitudes and energy.

INITIAL DATA

All earthquake catalogs used in this study were obtained from public sources. During the preparation step, the catalogs were stored in specialized databases and subjected to the standard procedure of primary analysis, which included checking the input data format, checking for duplicates, identifying and excluding aftershocks, estimating the representative magnitude, and analyzing its changes (Smirnov and Ponomarev, 2020).

Kamchatka Catalog

The regional catalog of Kamchatka earthquakes was obtained from the website of the Unified Seismological Data Information System of the Kamchatka Branch of the Federal Research Center "Unified Geophysical Survey of the Russian Academy of Sciences"[3]. The seismological observation system in Kamchatka and the above information system are described in the papers by (Chebrov et al., 2013; Chebrov et al., 2020). The information contained in the catalog is described on the website of the Unified Seismological Data Information System of the Kamchatka Branch of the Federal Research Center "Unified Geophysical Survey of the Russian Academy of Sciences"[4]. We downloaded the catalog of non–volcanic earthquakes (as classified in the Unified Seismological Data Information System of the Kamchatka Branch of the Federal Research Center "Unified Geophysical Survey of the Russian Academy of Sciences") for the entire observation period.

The energy characteristics in the Kamchatka catalog are given in energy classes, and the corresponding magnitude values are recalculated according to the correlation dependence. We used the initial values of the energy classes.

We examined the spatiotemporal variations of the class of completeness in the regional catalog of Kamchatka earthquakes in detail in the paper by (Smirnov et al., 2019). Figure 1 shows the change in the representative class over time from the paper by (Smirnov et al., 2019), supplemented with data for 2019–2023, as a general characteristic. The paper by (Smirnov et al., 2019) indicated that the representative class ranges from 6.5 to 9.5, depending on time and place, and exceeds the level $K_c = 9.5$ only at certain moments in time in the southernmost part of the region.

Japan Catalog

The regional catalog of Japan, as well as the Kamchatka catalog, was studied in detail for a magnitude of completeness estimate in the paper by (Smirnov et al., 2019). It stated the following: "Records from the International Seismological Center (ISC) catalog[5], which were provided by the Japan Meteorological Agency (JMA), were used as initial data. The catalog contains local magnitudes. The orthogonal regression of the values M_W from the Harvard centroid moment tensor catalog and the magnitude M from the JMA catalog that we selected gives the relationship $M_W = (0.98 \pm 0.02)M + (0.24 \pm 1)$, which is close to the relationship $M = M_W$. A magnitude of completeness analysis showed that, since 1981, events with $M \geq 3.3$. have been completely detected for the entire area".

Iceland Catalog

The regional catalog of Iceland is freely available on the website of the Icelandic Meteorological Office[6]. The catalog contains data from 1995 to 2023.

[3] https://sdis.emsd.ru/info/earthquakes/catalogue.php

[4] https://sdis.emsd.ru/info/earthquakes/catalogue.php?out=info

[5] ftp://isc-mirror.iris.washington.edu/pub/

[6] http://hraun.vedur.is/ja/viku/

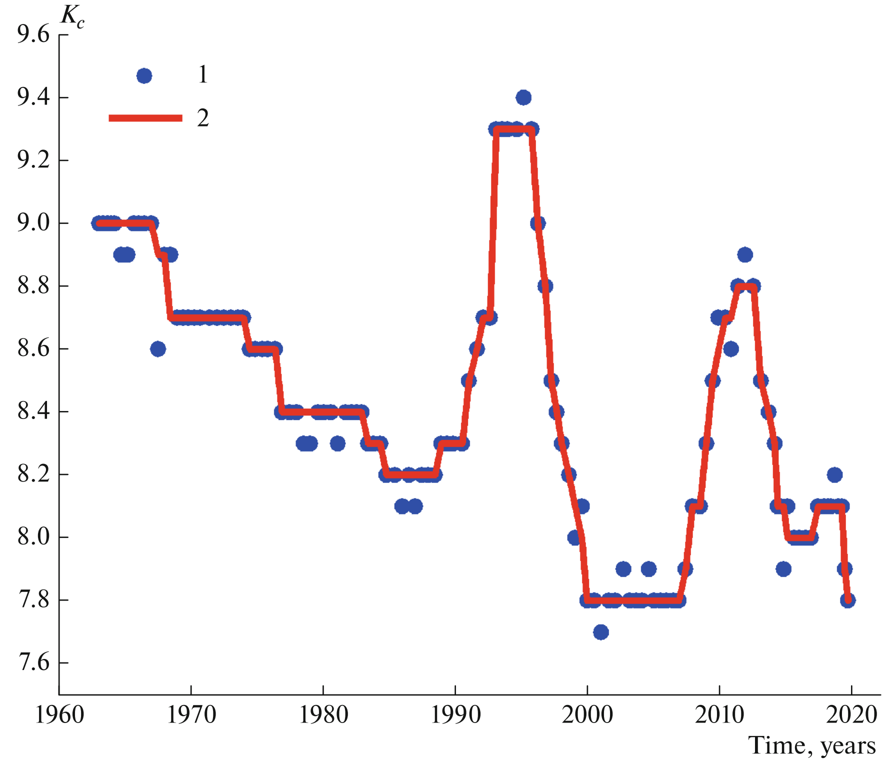

Fig. 1. A change in the class of completeness over time for the Kamchatka catalog: 1 are the initial estimates, 2 is the smoothed curve.

It has a total of over 500000 entries. The catalog lists local and moment magnitudes; we used the latter. The seismic network and the seismic service of Iceland are described in the paper by (Stefansson, 2011).

Figure 2 shows the change in the magnitude of completeness of the Iceland catalog over time. We can see that events with $M_W \geq 2.4$ can be considered representative of the entire observation interval. An analysis of the magnitude of completeness distribution in space indicates that this threshold is acceptable for the entire catalog.

RESULTS

Table 1 provides information about the selected earthquakes, and their location on the map is shown in Fig. 3. To ensure comparability, the energy class K from the catalog of Kamchatka earthquakes was recalculated to the moment magnitude M_w by formulas used in the Unified Seismological Data Information System of the Kamchatka Branch of the Federal Research Center "Unified Geophysical Survey of the Russian Academy of Sciences"[7]: $M_l = 0.5K - 0.75$ and $M_w = M_l - 0.4$.

[7] https://sdis.emsd.ru/info/earthquakes/catalogue.php?out=info&informationShow=show#Mw=f(Ml)

For each earthquake under study, we plotted maps of the RTL and b-value distribution in space at successive moments in time before the earthquake, and visually identified their pre–earthquake anomalies. Then, we plotted the curves of changes in the parameters over time for the central part of the anomaly. These curves were plotted up to one day before the date of the earthquake.

Catalog selection thresholds and calculation windows for the algorithms were varied for different earthquakes in order to obtain the most pronounced and stable anomalies (Tables 2 and 3). In choosing the threshold of selection by magnitude, we considered not only a general estimate of the catalog's representativeness, but also an estimate of the representative magnitude in the spatiotemporal vicinity of the respective earthquake. To calculate the RTL in formula (4), we set the p parameter equal to 1 in accordance with common practice (Sobolev and Ponomarev, 2003). It should be noted that, in a statistical sense, this value ensures the stability of the mean "energy release" estimate (Mikhailov et al., 2010; Smirnov and Zavyalov, 2012). From a physical point of view, the $p = 1$ value represents the sum of movements in the earthquake sources (taken as proportional to the rupture lengths) (Smirnov and Ponomarev, 2020). The value of the l_0 coefficient is not important in this implementation of the algo-

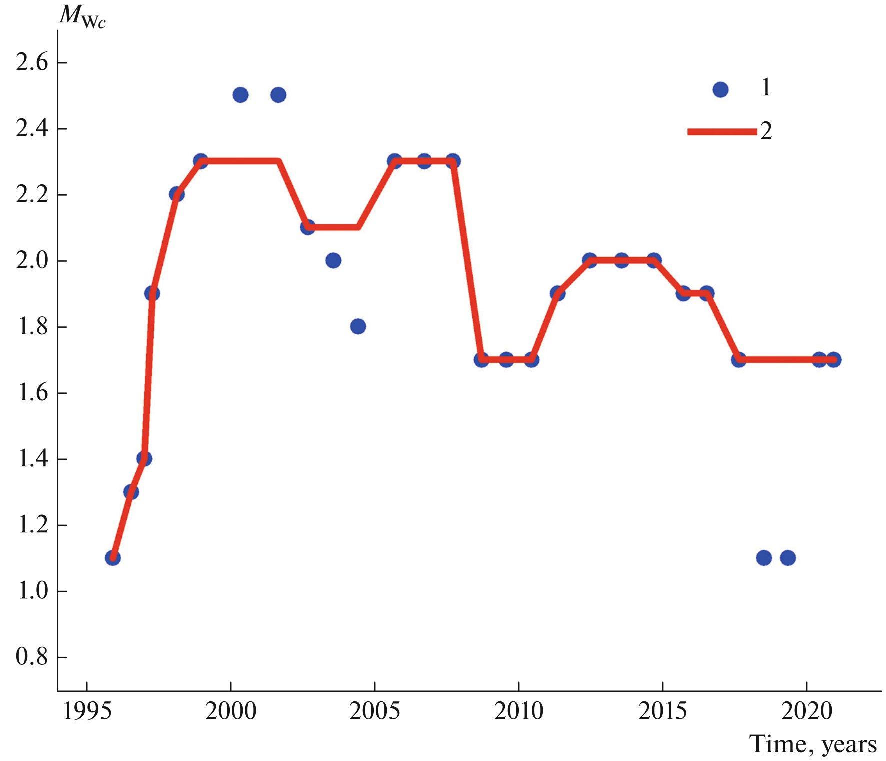

Fig. 2. A change in the magnitude of completeness over time for the Iceland catalog: 1 are the initial estimates, 2 is the smoothed curve.

rithm, because it introduces a straight line trend into (4), which is later removed before the *RTL* parameter is calculated.

Figures 4 and 5 show the distribution maps of the studied seismicity parameters at the moment of the largest anomaly value and the plots of parameter changes over time in the regions of the largest anomalies in the respective parameter. It should be noted that the regions of the largest *b* and *RTL* values in space do not always coincide. The time scale is given in years up

Table 1. Characteristics of earthquakes selected for analysis

Kamchatka	Date	Longitude	Latitude	Depth	Energy class (magnitude *Mw*)
1	Mar. 2, 1992	160.20	52.76	20	14.6 (6.2)
2	June 8, 1993	157.80	51.20	40	15.0 (6.4)
3	Nov. 12, 1993	158.83	51.79	40	14.6 (6.2)
4	Dec. 5, 1997	162.55	54.64	10	15.5 (6.6)
5	Feb. 20, 2011	162.47	55.73	49	14.1 (5.9)
6	Feb. 28, 2013	157.77	50.67	61	15.2 (6.5)
Japan	Date	Longitude	Latitude	Depth	Magnitude *Mw*
7	Oct. 4, 1994	147.68	43.37	28	8.1
8	Sept. 25, 2003	144.10	41.78	45	8.0
9	Mar. 11, 2011	142.86	38.10	24	9.1
Iceland	Date	Longitude	Latitude	Depth	Magnitude *Mw*
10	June 17, 2000	−20.37	63.975	6.35	5.5
11	May 29, 2008	−21.068	63.973	5.14	5.3
12	June 20, 2020	−18.551	66.254	10.01	5.6

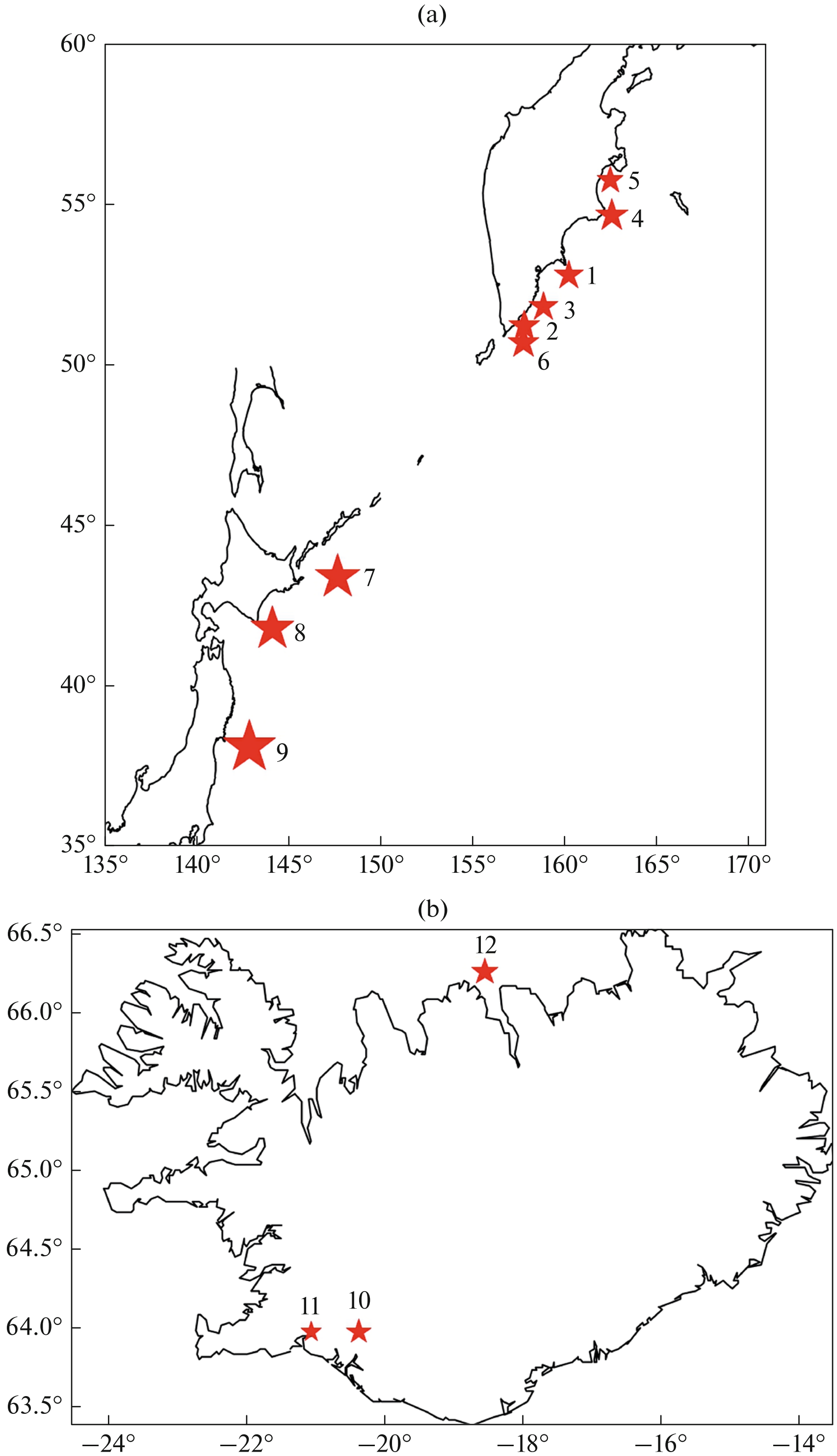

Fig. 3. Maps of the epicenters of the selected earthquakes: (a) Kamchatka and Japan; (b) Iceland. The size of the symbols is proportional to the magnitude, the numbers correspond to Table 1.

to the time of the respective earthquake. The *RTL* parameter is normalized to its long–term standard deviation (see the description of the *RTL* estimation procedure above). For the recurrence curve slope, instead of the *b*-value maps, Figs. 4 and 5 show maps of the *Z* parameter (formula (8)). This parameter takes into account both the values of *b*-value and their statistical errors compared to their long-term values. In this sense, the *Z* parameter is comparable to the *RTL* (which is also normalized to its long–term standard

Table 2. Catalog selection parameters and calculation windows of algorithms for Japan and Iceland earthquake analysis

Earthquake (date)	June 17, 2000	May 29, 2008	June 20, 2020	Oct. 4, 1994	Sept. 25, 2003	Mar. 11, 2011
RTL calculation parameters						
M_{min}	2	2	3	4.3	5	5
H_1, km	0	0	8	0	0	0
H_2, km	150	100	100	150	150	150
r_0, km	20	20	20	50	50	50
t_0, days	365	365	365	365	365	365
Time limit, days	700	700	700	700	700	700
Space limit, km	100	100	200	200	200	300
b-value calculation parameters						
M_{min}	1.8	1.5	1.5	4.5	4	5.4
H_1, km	0	0	0	0	0	0
H_2, km	150	150	8	150	200	200
Calculation window, number of events	200	200	200	110	110	110
Background window, number of events	600	600	400	330	330	330
Size of the calculation region, units of the source size	7	15	8	7	3	5

M_{min} is the threshold of selection by magnitude from below; H_1 and H_2 are the thresholds of selection by depth; r_0, t_0 are the parameters of the *RTL* algorithm (formulas (2) and (3)). *b*-value was calculated from formulas (6) and (7) in sliding windows containing a given number of events; the table shows the sizes of the working calculation windows and the background windows used to obtain an estimate of the parameter (formula (8)). The size of the spatial region has been given in the sizes of the principal earthquake source.

deviation), and its maps have greater contrast than the maps of the *b*-values.

Figures 4 and 5 also show curves of changes in the seismogenic rupture concentration parameter K_{sr} over time. This parameter was estimated in the selected spatial windows over the time interval up to the studied earthquake. According to the recommendations of (Zavyalov, 2006), the calculation of K_{sr} was started from the previous strong earthquake in the studied spatial region.

The red segments of the time plots in Figs. 4 and 5 show the *RTL* and *b*-value anomalies detected according to their "precursory patterns" Unlike the *RTL* and *b*-value, the K_{sr} value does not have a "precursory pattern". This is a cumulative parameter for which a critical value is empirically determined in prognostic studies and then used for prediction. The critical value is determined during the algorithm training step and is set by the K_{sr} value at the moment of the earthquake before which it is calculated. This critical value is used to select the level of K_{sr}, at which the alarm is triggered (Zavyalov, 2006). We did not use the ideology of the prognostic investigation in this paper. The K_{sr} parameter is important to us as an indicator of how close the failure regime is to avalanche–like increase conditions. We estimated the K_{sr} values, corresponding to the moments at which the *RTL* and *b* anomalies were formed. These estimates are given and discussed below.

DISCUSSION

According to the "precursory pattern", we assumed that the time at which the anomalies in the *RTL* and *b* parameters, highlighted in red in Figs. 4 and 5, began was the time at which the respective parameter started to decrease. The durations of the anomalies (time intervals from the beginning of the anomalies to the time of the earthquake) are given in Table 4 and graphically presented in Fig. 6.

Table 4 and Figure 6 show that the durations of the anomalies lie in the range from half a year to several years, which is typical of medium–term precursory anomalies (Sobolev, 1993; 2011). It should be noted that in prognostic studies, the "anomaly time" is often assumed to be the time from the anomaly maximum to the earthquake (Sidorin, 1992; Sobolev, 1993; 2011; Sobolev and Ponomarev, 2003). This is quite reasonable in prognostic studies as it helps to more reliably algorithmize the automatic detection of an anomaly. We will use our chosen definition of the duration of an anomaly from its beginning (rather than from its maximum) because we are interested in the physical aspect

Table 3. Catalog selection parameters and calculation windows of algorithms for Kamchatka earthquake analysis

Date	Mar. 2, 1992	June 8, 1993	Nov. 12, 1993	Dec. 5, 1997	Feb. 20, 2011	Feb. 28, 2013
RTL calculation parameters						
K_{min}	8.5	9	9	10	10	10
H_1, km	0	0	0	0	0	0
H_2, km	100	200	150	150	150	100
r_0, km	50	50	50	50	50	50
t_0, days	365	365	365	365	365	365
Time limit, days	700	700	700	700	700	700
Space limit, km	130	100	150	200	200	100
b-value calculation parameters						
K_{min}	8	8.5	8.5	9.4	8	8
H_1, km	0	0	0	0	0	0
H_2, km	200	200	200	200	200	200
Calculation window, number of events	100	100	100	180	100	100
Background window, number of events	500	400	400	540	300	500
Calculation region, units of the source size	5	6	6	8	3	3

The legend is the same as in Table 2.

Table 4. Durations of anomalies in *b*-value and *RTL* parameter and their difference

Region	Date	Magnitude	Duration of the *b-value* anomaly T_b, years	Duration of the *RTL* anomaly, T_{RTL}, years	$T_b - T_{RTL}$, years
Kamchatka	Mar. 2, 1992	6.2	1.42	1.71	–0.29
	June 8, 1993	6.4	4.55	2.56	1.99
	Nov. 12, 1993	6.2	4.77	3.52	1.25
	Dec. 5, 1997	6.6	2.04	1.31	0.73
	Feb. 20, 2011	5.9	2.74	2.57	0.17
	Feb. 28, 2013	6.5	2.42	2.17	0.25
	Median	**6.3**	**2.58**	**2.36**	**0.49**
Japan	Oct. 4, 1994	8.1	2.24	0.98	1.26
	Sept. 25, 2003	8.0	3.41	1.79	1.62
	Mar. 11, 2011	9.1	2.86	0.95	1.91
	Median	**8.1**	**2.86**	**0.98**	**1.62**
Iceland	June 17, 2000	5.5	1.3	0.44	0.86
	May 29, 2008	5.3	0.63	2.19	–1.56
	June 20, 2020	5.6	1.61	1.32	0.29
	Median	**5.5**	**1.3**	**1.32**	**0.29**

of anomaly formation, rather than the convenience of its use in practical earthquake prediction algorithms. If we compare our estimates from Table 4 with the "prognostic" anomaly durations, our estimates should be divided by about half.

The last column in Table 4 shows the difference between the durations of the *b* and *RTL* anomalies. We can see that this difference is positive for all but two earthquakes, i.e., the *b*-value anomaly occurs earlier than the *RTL* anomaly.

The selected earthquakes in the three regions have different magnitude ranges: 5.3–5.6 for Iceland, 5.9–6.6 for Kamchatka, and 8.0–9.1 for Japan. Figure 7 shows a summary of the mean anomaly durations and

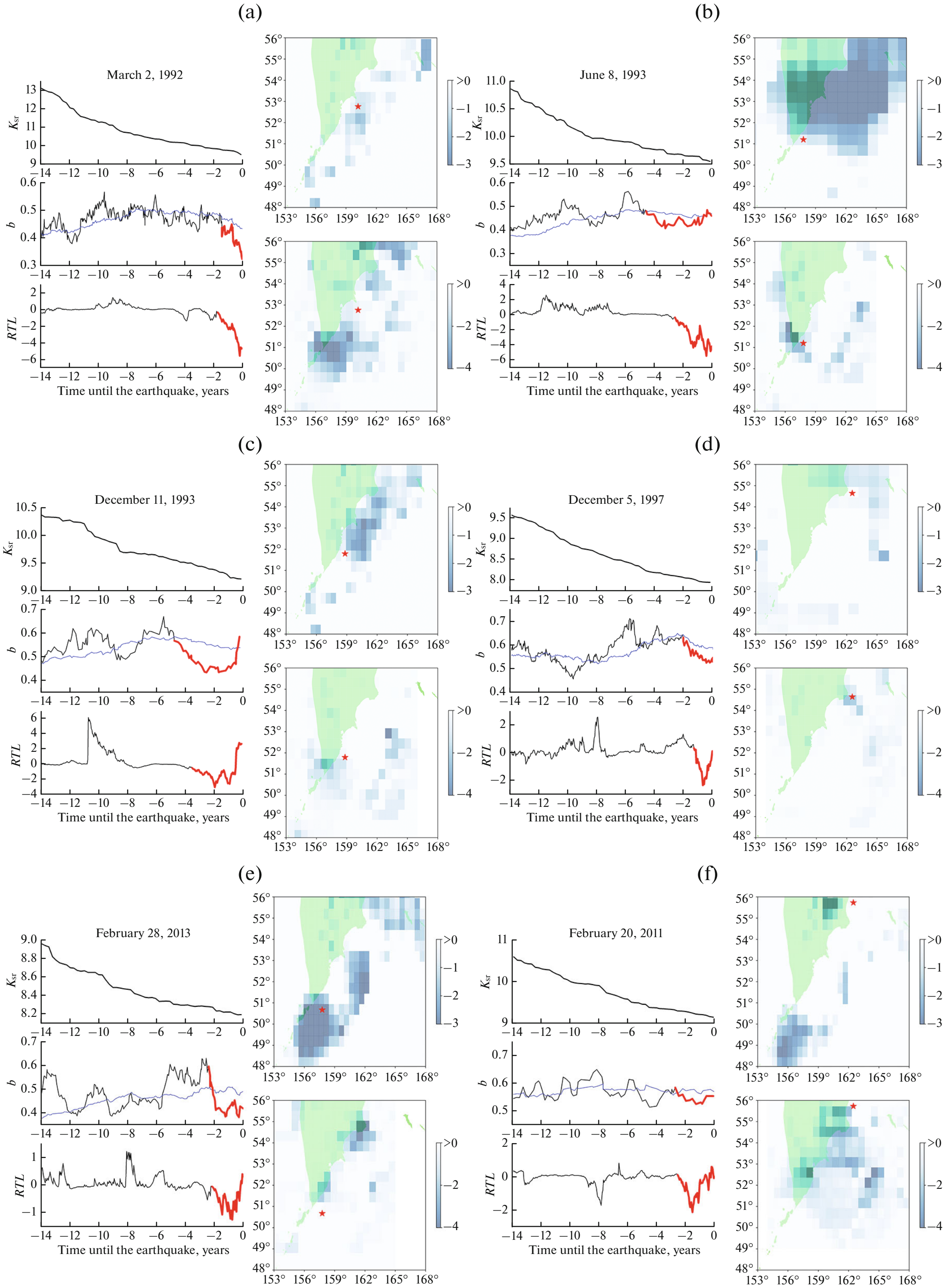

Fig. 4. Kamchatka: the distribution maps of the studied parameters of seismicity at the moment of the largest anomaly value and the plots of parameter changes over time. Maps: top—the parameter, bottom—the *RTL*; the star indicates the epicenter of the earthquake, the scale of the color range is shown to the right of the maps; (a)–(f) are various earthquakes; above the plots are their codes in the format year_month_day, the red segments indicate the anomalies. On the *b*-value plot, the thin line represents the values in the background windows.

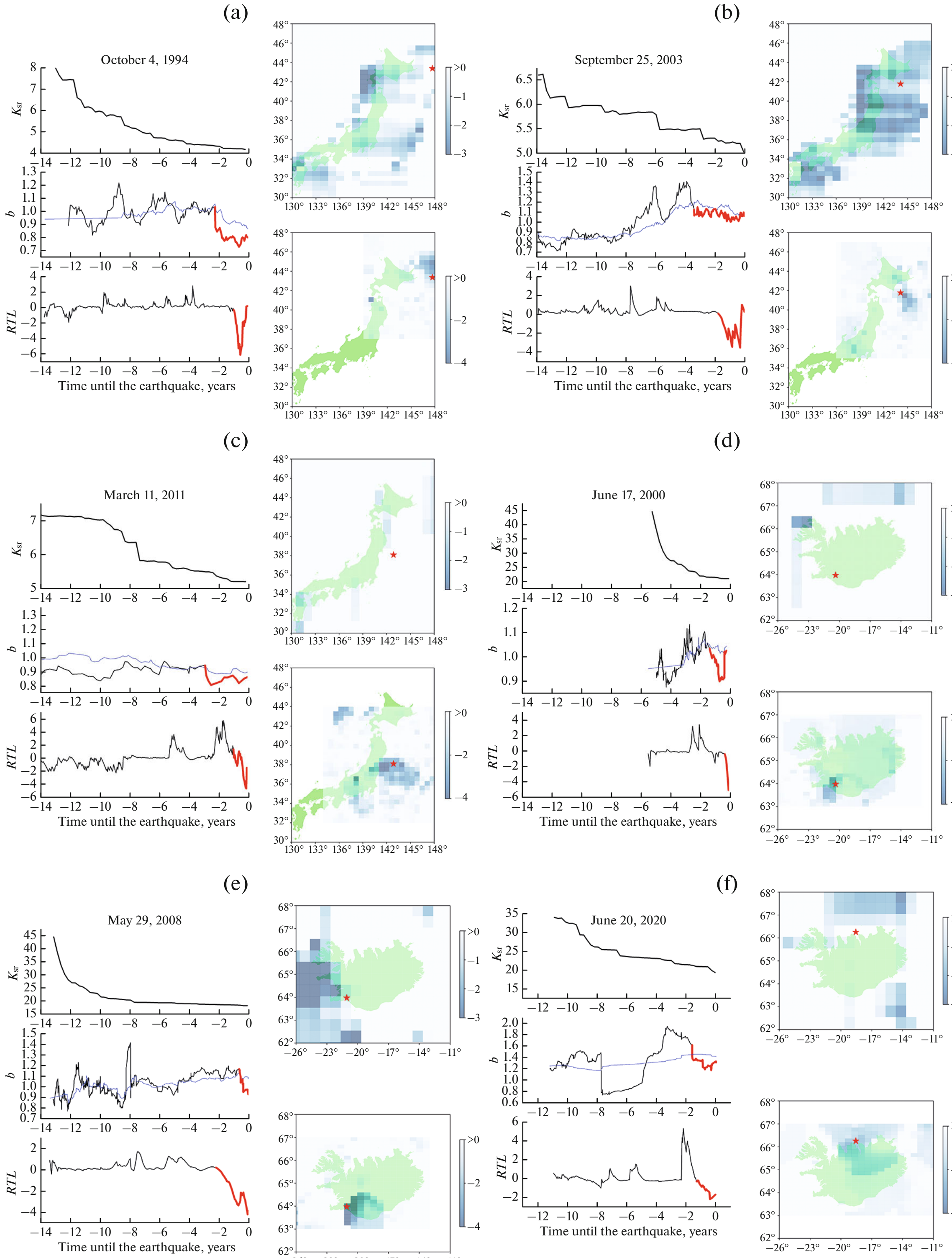

Fig. 5. Japan (a), (b), (c) and Iceland (d), (e), (f): the distribution maps of the studied parameters of seismicity at the moment of the largest anomaly value and the plots of parameter changes over time. The legend is the same as in Fig. 4.

their differences depending on the mean magnitude according to Table 4. We estimated mean durations using the median, which is a more robust estimate for small sample sizes.

Figure 7 shows that the durations of the *b*-value anomalies for the weakest earthquakes (Iceland) are shorter than those for the stronger earthquakes in Kamchatka and Japan. No systematic differences in

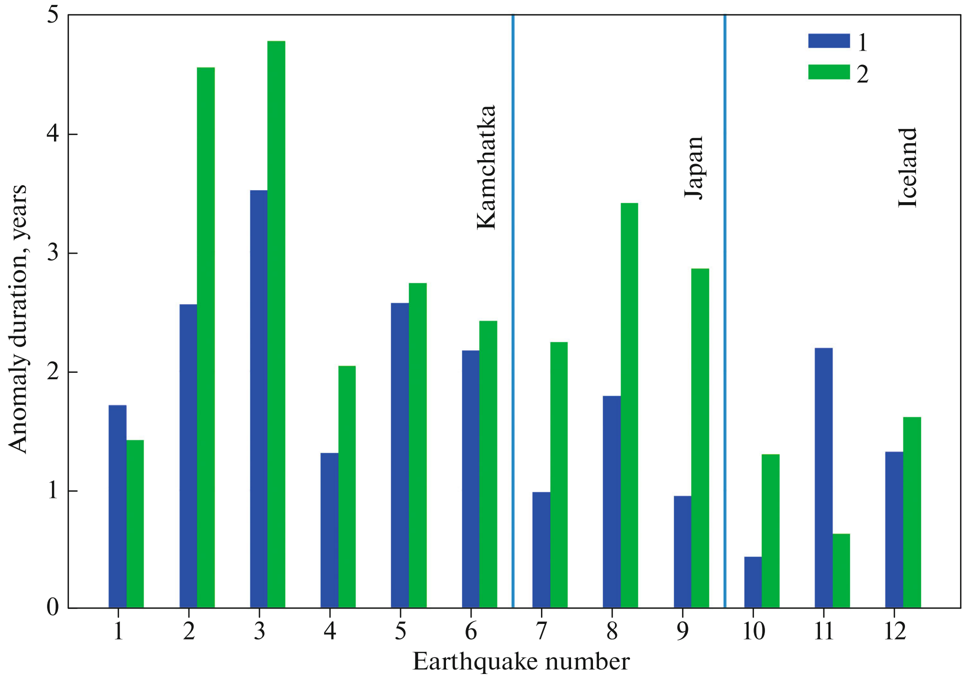

Fig. 6. Anomaly durations: *RTL* (1) and *b*-value (2), according to Table 4. The numbers of the earthquakes along the *x*–axis correspond to Table 1.

the durations of the *RTL* anomalies are observed. The difference between the durations of the *b* and *RTL* anomalies increases as the magnitude increases.

It should be noted that the small statistics of the studied earthquakes does not yet allow us to make a statistically valid conclusion about whether or not there is a difference in the durations of anomalies before earthquakes of different magnitudes. In addition, we cannot yet distinguish between the possible magnitude dependences of the anomaly parameters and their possible regional characteristics in the subduction zones (Kamchatka and Japan) and in the rift zone (Iceland).

As noted above, the seismogenic rupture concentration parameter can be used as an indicator of whether the system of accumulating ruptures is unstable. The K_{sr} value is essentially a ratio of the average distance between existing ruptures R to their average length l_{av}. Theoretically, two fractures on the same line lose stability when the ratio R/l_{av} is close to 2. This makes the theoretical critical value equal to $K_{sr}^* \approx 2$. Let us ask ourselves the question: at what K_{sr} values do the *b* and *RTL* anomalies occur?

The paper by (Smirnov and Zavyalov, 1996) shows that the estimates of the K_{sr} values and, therefore, the critical K_{sr}^* values at the time of the earthquake, obtained from formula (9), depend on the ratio between the size of the averaging cell and the size of the earthquake source. The index of this scale dependence is determined by the fractal dimensionality of the set of earthquake hypocenters. In particular, by varying the ratio of cell sizes and earthquake sources, the authors (Smirnov and Zavyalov, 1996) found that the critical K_{sr}^* values before the same earthquakes in the Kamchatka region change by more than three times.

To ensure the statistical validity of the estimates, we calculated the K_{sr} values for different earthquakes with different ratios of the cell size to the earthquake source. However, we did not estimate and did not take into account the scale dependence, so the K_{sr} values, corresponding to the beginning of the *b*-value and *RTL* anomalies for different earthquakes and for different regions, should not be compared. It is possible to compare the ratio of the K_{sr} values, corresponding to the beginning of the anomaly, to the critical K_{sr}^* value at the time of the principal earthquake. This ratio eliminates the dependence of estimate (9) on the size of the cell and the earthquake source. The corresponding ratios are shown in Table 5.

Table 5 shows that the K_{sr} values at the times when the *b*-value and *RTL* anomalies occur differ from the critical K_{sr}^* values (exceed them) on average by no more than 5%. The last column in Table 6 shows the range of K_{sr} variations within the corresponding seismic cycle—the ratio of K_{sr} at the beginning of the cycle

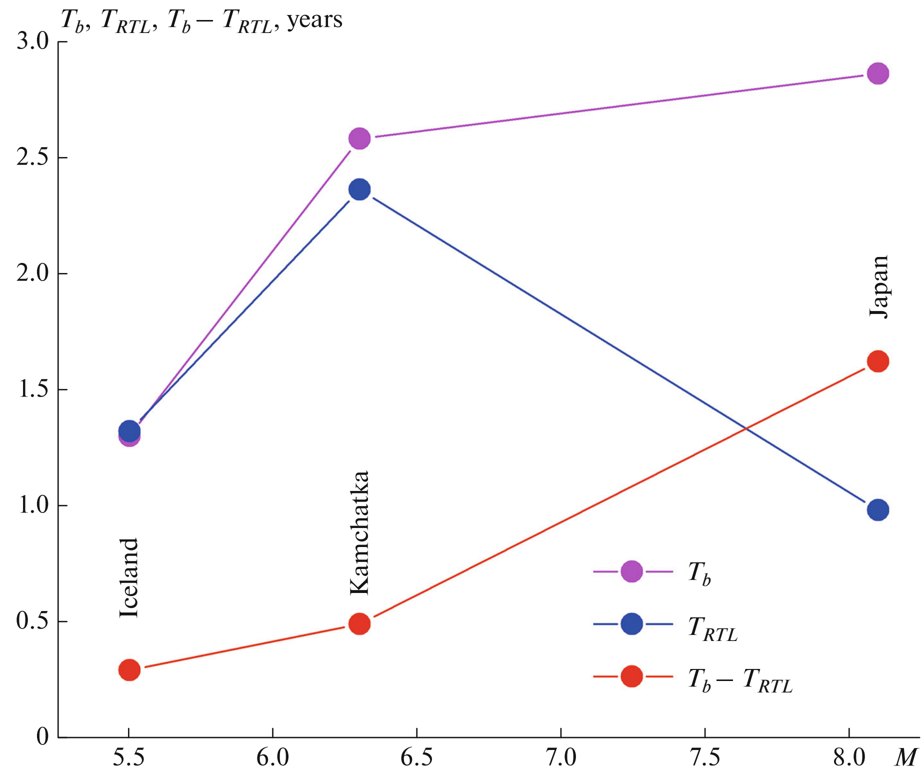

Fig. 7. The mean (median) durations of the b-value (T_b) and RTL (T_{RTL}) anomalies and their mean (median) difference (according to Table 5).

Table 5. Ratios of seismogenic rupture concentration values K_{sr} at the times b-value and RTL anomalies started and at the time the earthquake occurred

Region	Date	Magnitude	K_{sr}^{b}/K_{sr}^{*}	K_{sr}^{RTL}/K_{sr}^{*}	K_{sr}^{0}/K_{sr}^{*}
Kamchatka	Mar. 2, 1992	6.2	1.026	1.031	4.01
	June 8, 1993	6.4	1.025	1.014	6.55
	Nov. 12, 1993	6.2	1.037	1.029	4.87
	Dec. 5, 1997	6.6	1.015	1.009	4.89
	Feb. 20, 2011	5.9	1.019	1.016	4.42
	Feb. 28, 2013	6.5	1.010	1.009	7.63
Japan	Oct. 4, 1994	8.1	1.041	1.010	1.93
	Sept. 25, 2003	8.0	1.094	1.044	2.91
	Mar. 11, 2011	9.1	1.056	1.002	3.83
Iceland	June 17, 2000	5.5	1.026	1.002	2.14
	May 29, 2008	5.3	1.010	1.023	2.44
	June 20, 2020	5.6	1.098	1.083	4.00
Mean			**1.038**	**1.023**	**4.14**

K_{sr}^{*} is the critical K_{sr} value at the time the earthquake occurred; K_{sr}^{b} is the K_{sr} value at the time the b anomaly started; K_{sr}^{RTL} is the K_{sr} value at the time the RTL anomaly started; K_{sr}^{0} is the K_{sr} value at the beginning of the seismic cycle.

to K_{sr}. This ratio is on average about 4, i.e., 400%. Therefore, a difference of less than 5% between the K_{sr}^* values and the critical K_{sr}^* values can be considered small. This means that anomalies in the values of the *b* and *RTL* parameters occur when the seismogenic rupture concentration is close to the critical value.

CONCLUSIONS

By analyzing data from regional earthquake catalogs, we were able to detect seismicity anomalies before earthquakes of various magnitudes in regions with two general types of tectonics: in the subduction zone (Kamchatka and Japan catalogs) and in the rift zone (Iceland).

Comparing the durations of the anomalies in *b*-value and the *RTL* parameter, we found that they occur in stages. The *b* anomalies are generally observed earlier than the *RTL* anomalies. The question of why and how they are formed in stages is still unknown, but we will speculate on the subject.

The anomalies in *b*-value reflect changes in the energy spectrum of seismicity. A decrease in the *b*-values indicates an increasing proportion of stronger events and a decreasing proportion of weaker events. In terms of the physics of the source preparation process, in the context of AUF and similar fracture coalescence and growth concepts, this redistribution is associated with the formation of larger ruptures due to an increased interaction between the ruptures as their concentration increases, resulting from a greater overlap of stress field anomalies caused by the ruptures.

The *RTL* anomalies reflect the formation of seismic quiescences and the subsequent foreshock activation of seismicity. According to the AUF concept, the formation of seismic quiescences in the range of relatively weak earthquakes and the subsequent foreshock activation are associated both with a redistribution of the failure process from lower to higher scales and with the failure localization—the division of the metastable source region of a future earthquake into "passive" and "active" parts. The failure localization triggers an avalanche–like failure process in the weakened zone, the development of failures leads to a further decrease in the strength of this zone and, consequently, to a further avalanche–like activation of failures (Sobolev, 1993).

Our results indicate that the localization process occurs later than the energy spectrum of seismicity begins to change. It is possible that this delay increases as the earthquake magnitude increases, because we can see in Fig. 5 that the difference between the durations of the anomalies in *b*-value and the *RTL* increases as the earthquake magnitude increases.

Comparing the times at which seismicity anomalies (*b*-value and the *RTL*) occur with the values of the seismogenic rupture concentration parameter corresponding to these times indicates that the formation of seismicity anomalies occurs when the system of seismogenic ruptures has almost reached its critical value in the seismic cycle.

ACKNOWLEDGMENTS

This study is based on the data (regional catalog of Kamchatka earthquakes) obtained at the unique research facilities "Seismic infrasound array for monitoring Arctic cryolithozone and continuous seismic monitoring of the Russian Federation, neighboring territories and the world" (https://ckp-rf.ru/usu/507436/).

FUNDING

This study was funded by the Russian Science Foundation, Grant No. 23-27-00067 "Staging of seismicity anomalies manifestation before strong earthquakes ".

REFERENCES

Aki, K., Maximum likelihood estimate of *b* in the formula $\log N = a - bM$ and its confidence limits, *Bull. Earthquake Res. Inst., Univ. Tokyo*, 1965, vol. 43, pp. 237–239.

Chebrov, V.N., Droznin, D.V., Kugaenko, Yu.A., Levina, V.I., Senyukov, S.L., Sergeev, V.A., Shevchenko, Yu.V., and Yashchuk, V.V., The system of detailed seismological observations in Kamchatka in 2011, *J. Volcanol. Seismol.*, 2013, vol. 7, no. 1, pp. 16–36.
https://doi.org/10.1134/S0742046313010028

Chebrova, A.Yu., Chemarev, A.S., Matveenko, E.A., and Chebrov, D.V., Unified Seismological Data Information System of the Kamchatka Branch of the Federal Research Center "Unified Geophysical Survey of the Russian Academy of Sciences": organization principles, main elements and key functions, *Geofiz. Issled.*, 2020, vol. 21, no. 3, pp. 66–91.
https://doi.org/10.21455/gr2020.3-5

Kail, R., Zaytsev, A., and Burnaev, E., Recurrent convolutional neural networks help to predict location of earthquakes, *IEEE Geosci. Remote Sens. Lett.*, 2021, vol. 19, Article ID 8019005.

Kendall, M.D. and Stuart, A., *The Advanced Theory of Statistics, Vol. 2: Inference and Relationship*, London: Griffin, 1961.

Mikhailov, V.O., Nazaryan, A.N., Smirnov, V.B., Diament, M., Shapiro, N., Kiseleva, E.A., Tikhotskii, S.A., Polyakov, S.A., Smol'yaninova, E.I., and Timoshkina, E.P., Joint inversion of the differential satellite interferometry and GPS data: a case study of Altai (Chuia) earthquake of September 27, 2003, *Izv., Phys. Solid Earth*, 2010, vol. 46, no. 2, pp. 91–103.

Myachkin, V.I., Sobolev, G.A., Dolbilkina, N.A., Morozow, V.N., and Preobrazensky, V.B., The study of variations in geophysical fields near focal zones of Kamchatka, *Tectonophysics*, 1972, vol. 14, no. 3, pp. 287–293.

Mjachkin, V.I., Brace, W.F., Sobolev, G.A., and Dietrich, J.H., Two models for earthquake forerunners, *Pure Appl. Geophys.*, 1975, vol. 113, pp. 169–181.

Myachkin, V.I., Kostrov, B.V., Sobolev, G.A., and Shamina, O.G., Fundamentals of source physics and earthquake precursors, in *Fizika ochaga zemletryaseniya* (Physics of the Earthquake Source). Moscow: Nauka, 1975, pp. 6–29.

Nagao, T., Takeuchi, A., and Nakamura, K., A new algorithm for the detection of seismic quiescence: Introduction of the RTM algorithm, a modified RTL algorithm, *Earth, Planets Space*, 2011, vol. 63, pp. 315–324. https://doi.org/10.5047/eps.2010.12.007

Earthquakes and Sustainable Infrastructure, Panza, G.F., Kossobokov, V.G., Laor, E., and De Vivo, B., Eds., Amsterdam: Elsevier, 2021.

Petrushov, A.A. and Smirnov, V.B., *Svidetel'stvo o gosudarstvennoi registratsii programmy dlya EVM* (Computer Software State Registration Certificate), no. 2022611056, 2022.

Proskura, P., Zaytsev, A., Braslavsky, I., Egorov, E., and Burnaev, E., Usage of multiple RTL features for earthquakes prediction, in *Computational Science and Its Applications*, ICCSA 2019, Lecture Notes in Computer Science, vol. 11619, Cham: Springer, pp. 556–565. https://doi.org/10.1007/978-3-030-24289-3_41

Sadovsky, M. A., Pisarenko, V.F., and Steinberg, V.V., On the dependence of earthquake energy on the seismic focus volume, *Dokl. Akad. Nauk SSSR*, 1983, vol. 271, no. 3, pp. 598–602.

Saltykov, V.A. and Konovalova, A.A., Monitoring variations in the slope of the Kamchatka earthquake recurrence schedule: methods and examples, in *Problemy kompleksnogo geofizicheskogo monitorings Dal'nego Vostoka Rossii: Trudy Vtoroi regional'noi nauchno-tekhnicheskoi konf.* (Problems of Comprehensive Geophysical Monitoring in the Far East of Russia: Proc. 2nd Regional Scientific and Technical Conf.), Chebrov, V.N., Ed., Petropavlovsk-Kamchatskii, 2009, Petropavlovsk-Kamchatskii: GS RAN, 2010, pp. 235–238.

Saltykov, V.A., Kugaenko, Yu.A., Kravchenko, N.M., and Konovalova, A.A., A parametric representation of Kamchatka seismicity over time, *J. Volcanol. Seismol.*, 2013, vol. 7, no. 1, pp. 58–75.

Scholz, C.H., Sykes, L.R., and Aggarwal, Y.P., Earthquake prediction: a physical basis, *Science*, 1973, vol. 181, no. 4102, pp. 803–810.

Sidorin, A.Ya., *Predvestniki zemletryasenii* (Earthquake Peecursors), Moscow: Nauka, 1992.

Smirnov, V.B. and Ponomarev, A.V., *Fizika perekhodnykh rezhimov seismichnosti* (Physics of Seismicity Transient Modes), Moscow: RAN, 2020.

Smirnov, V.B. and Zavyalov, A.D., Incorporating the fractal distribution of faults as a measure of failure concentration, *J. Volcanol. Seismol.*, 1997, vol. 18, no. 4, pp. 447–452.

Smirnov, V.B. and Zavyalov, A.D., Seismic response to electromagnetic sounding of the Earth's lithosphere, *Izv., Phys. Solid Earth*, 2012, vol. 48, no. 7–8, pp. 615–639.

Smirnov, V.B., Ommi, S., Potanina, M.G., Mikhailov, V.O., Petrov, A.G., Shapiro, N.M., and Ponomarev, A.V., Estimates of lithospheric failure cycle parameters from regional earthquake catalogues, *Izv., Phys. Solid Earth*, 2019, vol. 55, no. 5, pp. 701–718.

Sobolev, G.A., *Fizicheskie osnovy prognoza zemletryasenii* (Physical Basis for Earthquake Prediction), Moscow: Nauka, 1993.

Sobolev, G.A., *Kontseptsiya predskazuemosti zemletryasenii na osnove dinamiki seismichnosti pri triggernom vozdeistvii* (The Concept of Earthquake Predictability Based on the Dynamics of Seismicity under Trigger Effect), Moscow: IFZ RAN, 2011.

Sobolev, G.A., Avalanche unstable fracturing formation model, *Izv., Phys. Solid Earth*, 2019, vol. 55 no. 1, pp. 138–151.

Sobolev, G.A. and Ponomarev, A.V., *Fizika zemletryasenii i predvestniki* (Earthquake Physics and Precursors), Moscow: Nauka, 2003.

Sobolev, G.A. and Zavyalov, A.D., A concentration criterion for seismically active faults, *Dokl. Akad. Nauk SSSR*, 1980, vol. 252, no. 1, pp. 69–71.

Sobolev, G.A., Tyupkin, Yu.S., Smirnov, V.B., and Zavyalov, A.D., Method of medium–term earthquake prediction, *Dokl. Akad. Nauk*, 1996, vol. 347, no. 3, pp. 405–407.

Stefánsson, R., *Advances in Earthquake Prediction*, Berlin: Springer, 2011.

Zavyalov, A.D., *Srednesrochnyi prognoz zemletryasenii: osnovy, metodika, realizatsiya* (Medium-Term Earthquake Forecasting: Basic Principles, Methods, Implementation), Moscow: Nauka, 2006.

Zhang, Y. and Huang, Q., Seismicity changes before major earthquakes in Sichuan, China, revealed by a combination of the RTL algorithm and ETAS model, *Seismol. Res. Lett.,* 2023, vol. 94, no. 2A, pp. 844–851. https://doi.org/10.1785/0220220282

Zhurkov, S.N., Kuksenko, V.S., Petrov, V.A., Savel'ev, V.N., and Sultonov, U.S., On prediction of rock failure, *Izv. Akad. Nauk SSSR, Fiz. Zemli*, 1977, no. 6, pp. 11–18.

Zhurkov, S.N., Kuksenko, V.S., Petrov, V.A., Savel'ev, V.N., and Sultanov, U.S., Concentration criterion for volumetric fracture of solids, in *Fizicheskie protsessy v ochagakh zemletryasenii* (Physical Processes in Earthquake Sources), Sadovskii, M.A. and Myachkin, V.I., Eds., Moscow: Nauka, 1980, pp. 78–86.